


# Annealing effect on structural and optical properties of glancing angle synthesized Gd<sub>2</sub>O<sub>3</sub> nanorod

Ph. Nonglen Meitei<sup>1</sup> · Naorem Khelchand Singh<sup>1</sup>

Received: 30 January 2023 / Accepted: 7 March 2023

Published online: 10 March 2023

© The Author(s) 2023 

## Abstract

Gadolinium oxide nanorod (Gd<sub>2</sub>O<sub>3</sub> NR) was fabricated on an n-type silicon substrate by catalyst-free glancing angle deposition (GLAD) technique. The as-grown sample was annealed at 500 °C to investigate the impact of annealing on structure and optical properties. XRD analysis reveals an improvement in the crystal structure after annealing. Field emission scanning electron microscope (FE-SEM) and energy dispersive X-ray (EDX) confirm the successful growth of vertically aligned Gd<sub>2</sub>O<sub>3</sub> NR with the presence of Gd, O, and Si. Transmission electron microscope (TEM) showed the crystalline nature of the grown Gd<sub>2</sub>O<sub>3</sub> NR. Finally, UV–vis spectroscopy was performed to study the optical properties. A significant enhancement in the photon absorption (200–300 nm) was observed, which can be attributed to increased grain size, improved crystallinity, and large generation of electron–hole pairs. In addition, the Tauc plot showed a decrease in the bandgap from 5.05 eV to 4.98 eV after annealing at 500 °C.

**Keywords** Gadolinium oxide · Nanorod · Annealing · Glancing angle deposition

## 1 Introduction

Semiconducting oxide has gained considerable attention in recent decades due to its promising technological applications in sensors, storage, and optoelectronic devices [1, 2]. Among these semiconducting oxides, gadolinium oxide (Gd<sub>2</sub>O<sub>3</sub>), a rare earth material, is a good candidate for various applications such as memory devices and photodetectors due to its wide bandgap material with high thermal stability and dielectric constant [3]. Recently, nanostructures such as zero-dimensional (0D), one-dimensional (1D), and two-dimensional (2D) have attracted particular attention due to their unique properties and potential for innovative applications [4–7]. Among the different types of nanostructures, 1D nanostructures such as nanowires and nanorods (NR) have received particular attention due to the large surface-to-volume ratio and quantum confinement effect [8]. A variety of techniques, including chemical methods [9] and physical vapour deposition (PVD) [10], have been employed for the deposition of metal oxide 1D nanostructures. Among these techniques, glancing angle deposition (GLAD) is an efficient method of growing vertically aligned NRs on a Si substrate without a catalyst. Also, the GLAD technique provides an easy way to control the NR's thickness, morphology, and porosity [11]. However, structural deformation during the deposition process, such as surface defects, adsorbed oxygen, and oxygen vacancies, can greatly affect the performance of optoelectronic devices. One way to reduce such defects is through heat treatment. Annealing the sample at optimal temperature reduces the structural defects and improves the crystallinity of the sample [12].

✉ Ph. Nonglen Meitei, nonglenm@gmail.com | <sup>1</sup>Department of Electronics and Communication Engineering, National Institute of Technology, Dimapur 797103, Nagaland, India.



**Fig. 1** Diagram illustrating the synthesis of  $\text{Gd}_2\text{O}_3$  nanorod

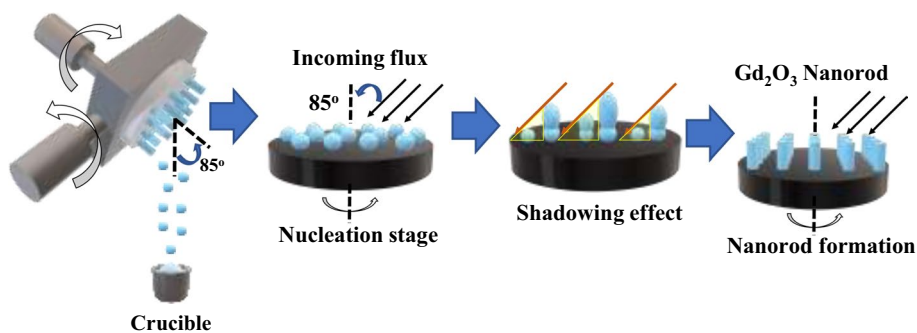
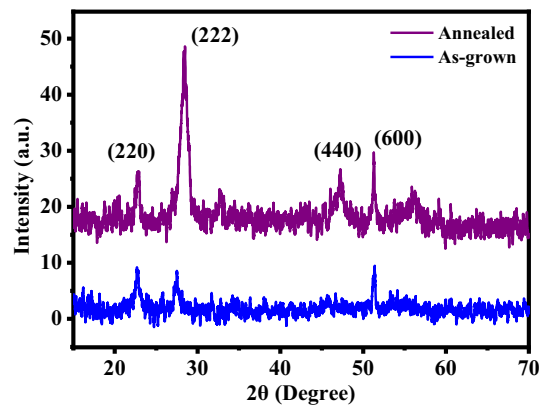


**Fig. 2** XRD patterns of as-grown and annealed  $\text{Gd}_2\text{O}_3$  NR



The optical and structural properties of  $\text{Gd}_2\text{O}_3$  nanoparticles have already been reported by other researchers. However, studies of these properties for  $\text{Gd}_2\text{O}_3$  NR using the GLAD technique are less explored. Therefore, in this study, we deposited  $\text{Gd}_2\text{O}_3$  NR on a Si substrate using the GLAD technique. Also, post-annealing at  $500^\circ\text{C}$  was performed to investigate the effect of annealing on  $\text{Gd}_2\text{O}_3$  NR properties. The structural analysis was carried out using an X-ray diffractometer (XRD), field-emission gun scanning electron microscope (FEGSEM), energy dispersive X-ray (EDX), and transmission electron microscope (TEM). The optical analysis was carried out using a UV–Vis spectrometer.

## 1.1 Experimental details

The GLAD technique was used to deposit  $\text{Gd}_2\text{O}_3$  (99.99% purity) NR on an n-type Si substrate. The substrate was first subjected to RCA cleaning procedure. The cleaned substrate was then placed on the substrate holder at an angle of  $85^\circ$  from the source materials. The deposition was carried out in a vacuum environment with a base pressure of  $\sim 5.5 \times 10^{-6}$  mbar, a deposition rate of  $1.1 \text{ \AA/s}$ , and an azimuthal rotation of 30 rpm. The length of the NR was monitored using a digital thickness monitor (DTM). After the deposition, the samples were subjected to open-air annealing at  $500^\circ\text{C}$  for 1 h in the programmable furnace. Figure 1 illustrates the synthesis of  $\text{Gd}_2\text{O}_3$  NR using the GLAD technique.

## 2 Result and discussions

Figure 2 shows the XRD patterns of the as-grown and annealed  $\text{Gd}_2\text{O}_3$  NR samples. The diffraction peak obtained for both samples matched the cubic phase with JCPDS data 65–3181. However, the (222) peak in the as-grown sample showed a slight shift due to strain developed during the deposition. After annealing at  $500^\circ\text{C}$ , the shifted peak returned to its original position, and a new peak with a (440) orientation plane appeared. The increasing peak intensity in the dominant (222) peak indicates an improved crystalline structure after annealing. The average crystallite size was calculated as  $\sim 18.05 \text{ nm}$  (as-grown) and  $\sim 21.85 \text{ nm}$  (annealed) using Scherrer's equation [2].

Figures 3 (a, b) present the FESEM image of the cross-sectional and top-view for the as-grown  $\text{Gd}_2\text{O}_3$  NR. The cross-sectional image confirms the successful growth of vertically aligned  $\text{Gd}_2\text{O}_3$  NR with  $\sim 300$  nm length. Some undergrown NRs are also observed due to the shadowing effect of the GLAD technique. Figure 3 (c–f) shows the EDX spectrum and elemental mapping of  $\text{Gd}_2\text{O}_3$  NR. The presence of O, Gd, and Si confirms the formation of good quality and impurity-free thin film, which is consistent with the XRD and SEM results.

Figure 4 (a) shows a single as-grown  $\text{Gd}_2\text{O}_3$  NR with  $\sim 310$  nm length, indicating the successful growth of NR. The d-spacing calculated from the HRTEM (Fig. 4 (b)) was found to be 0.311 nm corresponding to the dominant peak with the (222) plane. Furthermore, the presence of lattice fringes confirms the crystalline nature of the as-grown sample. Figure 4 (c) shows a single annealed  $\text{Gd}_2\text{O}_3$  NR with  $\sim 275$  nm length. The nanorod in the annealed sample became smoother due to grain agglomeration and exhibited better crystallinity with a larger diameter, as shown in Figs. 4 (a, c). The improvement in the crystallinity after annealing is well-matched with the XRD analysis.

UV–Vis spectra of the as-grown and annealed  $\text{Gd}_2\text{O}_3$  NR are shown in Fig. 5 (a). A maximum absorption in the UV region (200–300 nm) was observed due to band-to-band transition [13]. It can be observed that the absorption of the sample increases in the annealed sample. The increased absorption in the annealed sample can be attributed to the generation of more electron and hole pairs and the improvement in the average crystallite size and crystallinity [14]. From the inset, we can observe a slight red shift in the absorption edge from the as-grown to the annealed sample, which can be attributed to changes in the particle size (due to grain agglomeration) and surface microstructure of the

**Fig. 3** **a** As-grown Cross-sectional FEGSEM image **b** As-grown top-view FEGSEM image **c** EDX spectrum (**d–f**) elemental mapping of O, Gd, and Si

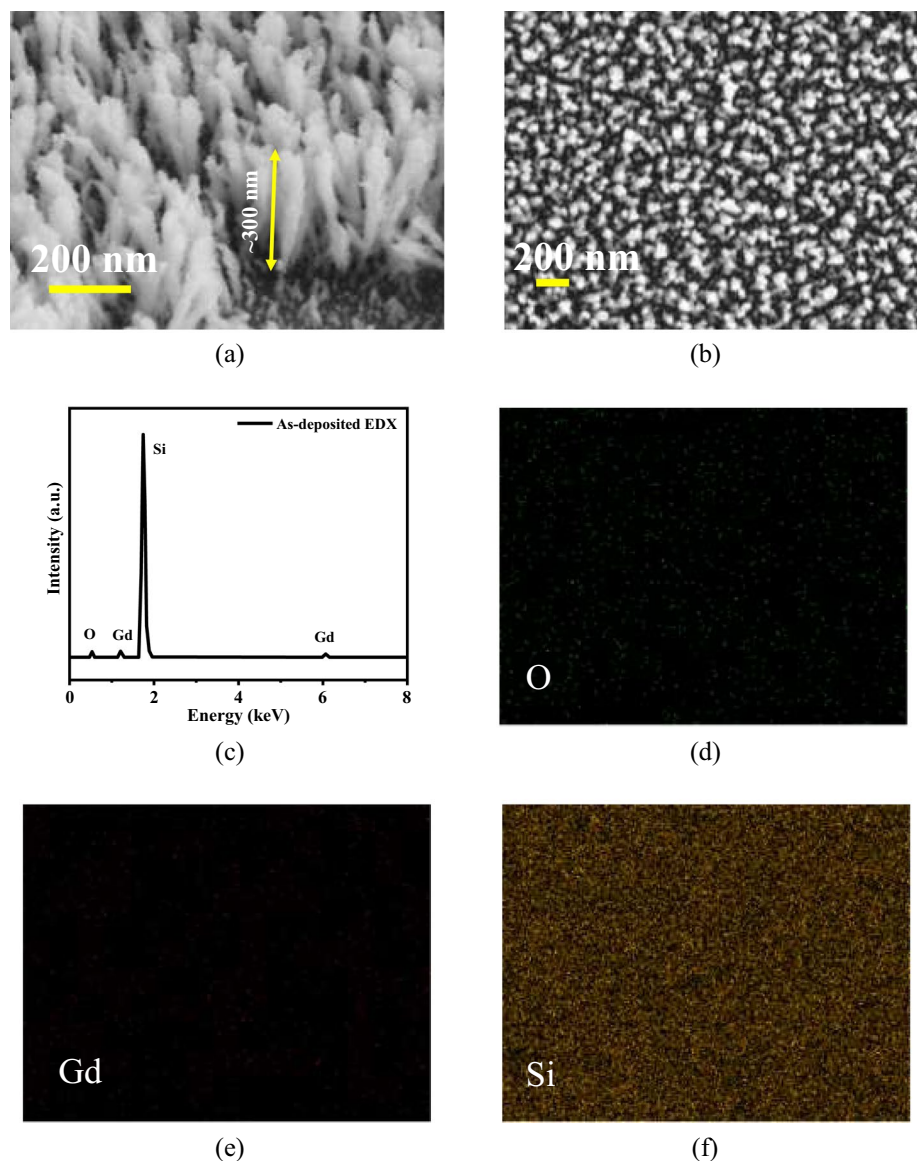


**Fig. 4** **a** Single as-grown  $\text{Gd}_2\text{O}_3$  NR **b** HRTEM image of as-grown  $\text{Gd}_2\text{O}_3$  NR **c** Single annealed  $\text{Gd}_2\text{O}_3$  NR **d** HRTEM image of annealed  $\text{Gd}_2\text{O}_3$  NR

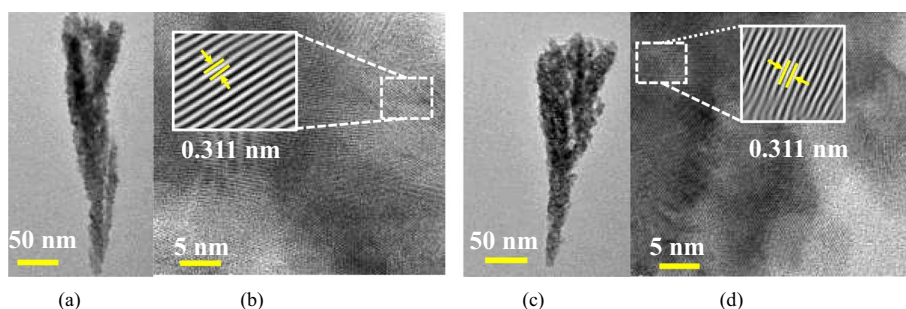
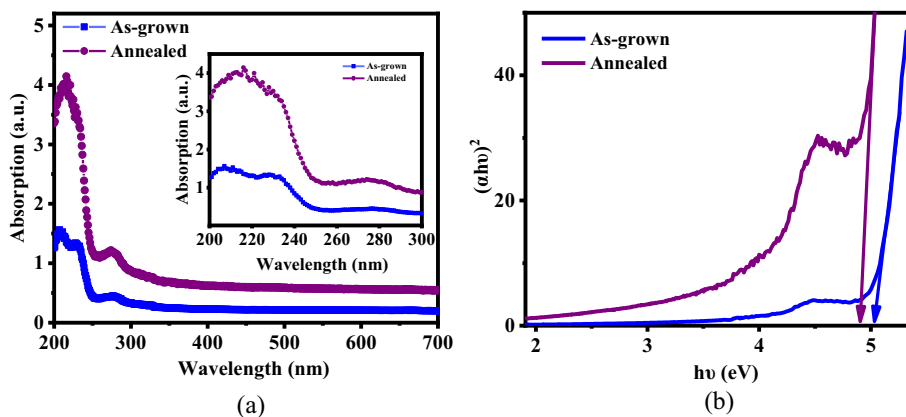


**Fig. 5** **a** Optical absorption. Inset shows the magnified view of the absorption spectra **b** Tauc plot of as-grown and annealed  $\text{Gd}_2\text{O}_3$  NR



NR after annealing. The optical band gap was calculated using the Tauc plot [13] given by  $(\alpha h\nu) \propto (h\nu - E_g)^{1/n}$  where  $h\nu$  = photon energy,  $E_g$  = bandgap,  $\alpha$  = absorption coefficient, and  $n = 2$  for direct transition. As shown in Fig. 5 (b), the result of extrapolating the  $(\alpha h\nu)^2 = 0$  the bandgap was found to be 5.05 eV (as-grown) and 4.98 eV (annealed).

### 3 Conclusion

In this study, we present the deposition of  $\text{Gd}_2\text{O}_3$  NR using the GLAD technique. The annealing effect on the structural and optical properties was studied. The XRD analysis confirms the improved crystallinity after annealing with an average crystallite size of  $\sim 18.05$  nm (as-grown) and  $\sim 21.85$  nm (annealed). FEGSEM and EDX analysis show the successful growth of good quality  $\text{Gd}_2\text{O}_3$  NR. TEM analysis confirms the improved crystallinity after annealing. Finally, the optical absorption of the annealed sample showed enhancement compared to the as-grown sample with an optical bandgap of 5.05 eV (as-grown) and 4.98 eV (annealed).

**Acknowledgements** The authors would like to acknowledge coe-am NIT Durgapur, SAIF, NEHU and NIT Nagaland for FEGSEM, TEM, XRD and UV-Vis measurement.

**Author contributions** NM did the preliminary literature review. The fabrication, characterization and analysis of result was done by Ph. Nonglen Meitei and Naorem Khelchand Singh. Finally the preparation of the manuscript was done by NM and NK Singh. All the authors read and approved the final manuscript.

**Funding** No funding was received for conducting the study.

**Data availability** The data that support the findings of this study are available within the article.

**Code availability** Not applicable.

## Declarations

**Competing interests** On behalf of all authors, the corresponding authors state that there is no competing interest.

**Open Access** This article is licensed under a Creative Commons Attribution 4.0 International License, which permits use, sharing, adaptation, distribution and reproduction in any medium or format, as long as you give appropriate credit to the original author(s) and the source, provide a link to the Creative Commons licence, and indicate if changes were made. The images or other third party material in this article are included in the article's Creative Commons licence, unless indicated otherwise in a credit line to the material. If material is not included in the article's Creative Commons licence and your intended use is not permitted by statutory regulation or exceeds the permitted use, you will need to obtain permission directly from the copyright holder. To view a copy of this licence, visit <http://creativecommons.org/licenses/by/4.0/>.

## References

1. Talapin DV, Gaponik N, Borchert H, Rogach AL, Haase M, Weller H. Etching of colloidal InP nanocrystals with fluorides: photochemical nature of the process resulting in high photoluminescence efficiency. *J Phys Chem B*. 2002;106:12659–63. <https://doi.org/10.1021/jp026380n>.
2. Meitei PhN, Alam MW, Ngangbam C, Singh NK. Enhanced UV photodetection characteristics of annealed Gd<sub>2</sub>O<sub>3</sub> nanorods. *Appl Nanosci*. 2021;11:1437–45. <https://doi.org/10.1007/s13204-021-01787-7>.
3. Yang Z, Yang L, Dai B, Lei P, Guo S, Wang P, et al. Evolution of microstructures and optical properties of gadolinium oxide with oxygen flow rate and annealing temperature. *J Rare Earths*. 2019;37:410–5. <https://doi.org/10.1016/j.jre.2018.09.006>.
4. Ikram M, Haider A, Bibi ST, Ul-Hamid A, Haider J, Shahzadi I, et al. Synthesis of Al/starch co-doped in CaO nanoparticles for enhanced catalytic and antimicrobial activities: experimental and DFT approaches. *RSC Adv*. 2022;12:32142–55. <https://doi.org/10.1039/D2RA06340A>.
5. Moeen S, Ikram M, Haider A, Haider J, Ul-Hamid A, Nabgan W, et al. Comparative study of sonophotocatalytic, photocatalytic, and catalytic activities of magnesium and chitosan-doped tin oxide quantum dots. *ACS Omega*. 2022;7:46428–39. <https://doi.org/10.1021/acsomega.2c05133>.
6. Ikram M, Haider A, Imran M, Haider J, Naz S, Ul-Hamid A, et al. Assessment of catalytic, antimicrobial and molecular docking analysis of starch-grafted polyacrylic acid doped BaO nanostructures. *International J Biol Macromol*. 2023. <https://doi.org/10.1016/j.ijbiomac.2023.123190>.
7. Nonglen Meitei Ph, Singh NK. Effect of annealing on forming-free bipolar resistive switching of Gd<sub>2</sub>O<sub>3</sub> thin films. *J Alloys Comp*. 2023. <https://doi.org/10.1016/j.jallcom.2023.168900>.
8. Xiang X, Cao C-B, Zhu H-S. Synthesis and photoluminescence of gallium oxide ultra-long nanowires and thin nanosheets. *J Cryst Growth*. 2005;279:122–8. <https://doi.org/10.1016/j.jcrysgro.2005.02.022>.
9. Vergés MA, Mifsud A, Serna CJ. Formation of rod-like zinc oxide microcrystals in homogeneous solutions. *J Chem Soc Faraday Trans*. 1990;86:959–63. <https://doi.org/10.1039/FT9908600959>.
10. Yao BD, Chan YF, Wang N. Formation of ZnO nanostructures by a simple way of thermal evaporation. *Appl Phys Lett*. 2002;81:757–9. <https://doi.org/10.1063/1.1495878>.
11. Rajkumari R, Ngangbam C, Singh NK. Presence of capacitive memory in GLAD-synthesized WO<sub>3</sub> nanowire. *J Mater Sci: Mater Electron*. 2021;32:3191–200. <https://doi.org/10.1007/s10854-020-05067-y>.
12. Meitei PhN, Moirangthem B, Ngangbam C, Alam MW, Singh NK. Investigation on structural and photodetection properties of Gd<sub>2</sub>O<sub>3</sub> thin films after annealing. *J Mater Sci Mater Electron*. 2022;33:10705–14. <https://doi.org/10.1007/s10854-022-08053-8>.
13. Dhananjaya N, Nagabhushana H, Nagabhushana BM, Rudraswamy B, Sharma SC, Sunitha DV, et al. Effect of different fuels on structural, thermo and photoluminescent properties of Gd<sub>2</sub>O<sub>3</sub> nanoparticles. *Spectrochim Acta Part Mol Biomol Spectrosc*. 2012;96:532–40. <https://doi.org/10.1016/j.saa.2012.04.067>.
14. Chetri P, Dhar JC. Improved photodetector performance of SnO<sub>2</sub> nanowire by optimized air annealing. *Semicond Sci Technol*. 2020. <https://doi.org/10.1088/1361-6641/ab7434>.

**Publisher's Note** Springer Nature remains neutral with regard to jurisdictional claims in published maps and institutional affiliations.